ELSEVIER

Physics of the Earth and Planetary Interiors 119 (2000) 3–23

PHYSICS OF THE EARTH AND PLANETARY INTERIORS

www.elsevier.com/locate/pepi

The COSY Project: verification of global seismic modeling algorithms

Heiner Igel [a,*], Nozomu Takeuchi [b,1], Robert J. Geller [b], Charles Megnin [c], Hans-Peter Bunge [d], Eric Clévédé [e], Jörg Dalkolmo [f], Barbara Romanowicz [c]

[a] *Institute of Theoretical Geophysics, University of Cambridge, Cambridge, UK*
[b] *Department of Earth and Planetary Science, Graduate School of Science, University of Tokyo, Tokyo, Japan*
[c] *Berkeley Seismological Observatory, University of California, Berkeley, CA, USA*
[d] *Department of Earth Sciences, Princeton University, Princeton, NJ, USA*
[e] *Institut de Physique du Globe, University of Paris, Paris, France*
[f] *Institute of Geophysics, University of Stuttgart, Stuttgart, Germany*

Received 20 April 1999; received in revised form 8 October 1999; accepted 19 October 1999

Abstract

Progress in determining the details of the global 3-D seismic velocity structure requires the ability to accurately model seismic wave propagation (e.g., travel times, waveforms, etc.) through heterogeneous 3-D Earth models. While for spherically symmetric models (quasi-) analytical solutions are available for the verification of numerical algorithms, this is not the case for general heterogeneous models. It is therefore desirable to establish global 3-D test models and verified reference seismograms, which allow us to assess the accuracy of numerical algorithms quantitatively. Prior to a workshop held on this issue at the 1997 IASPEI Meeting, a 3-D test model was handed out to various groups and long-period synthetic seismograms were returned. This workshop was the initiation of the COmparison of global SYnthetic seismogram techniques (COSY) Project, which aims at establishing a WWW page (http://www.geophysik.uni-muenchen.de/COSY), where the test models and seismograms as well as some of the algorithms can be accessed. In this paper, we study the accuracy of and compare solutions from different numerical methods for a spherically symmetric model and the 3-D test model. The algorithms compared use the normal-mode method, the Direct Solution Method (DSM), a direct evaluation of the Greens function for spherically symmetric media (GEMINI), and the finite-difference (FD) method. Our 3-D test model is a perturbation to the spherically symmetric background model (PREM) based on a (scaled) temperature field from numerical modeling of mantle convection. The model displays many features in common with recent seismic tomographic images. We suggest that in addition to (future) 3-D reference Earth models, verified reference synthetic seismograms should be established for use by the seismological community.

Keywords: COSY Project; Seismic modeling algorithms; 3-D Earth models

* Corresponding author. Institut für Angewandte und Allgemeine Geophysik, Ludwig-Maximilians University, Theresienstrasse 41, 80333 Munich, Germany. Tel.: +49-8923944204; fax: +49-8923944205; e-mail: igel@geophysik.uni-muenchen.de

[1] Present address: Earthquake Research Institute, University of Tokyo, Tokyo, Japan.

0031-9201/00/$ - see front matter
PII: S0031-9201(99)00150-8

1. Introduction

Global seismology aims at finding the Earth model with the best overall fit to the enormous amount of recorded data that is available today. This data set is growing at an almost exponential rate. The information contained in the whole spectrum of modern seismic broadband recordings exceeds by far what we are able to model or resolve with present simulation algorithms, receiver coverage and inversion techniques. While the station coverage is becoming denser, and the ocean bottoms are being instrumented with permanent recording equipment, computational seismologists are advancing the development of algorithms that allow the simulation of wave propagation through anelastic, anisotropic, fully heterogeneous models on a global scale.

Most of the geodynamical questions to be resolved today are directly related to seismic heterogeneity and/or anisotropy in the Earth's deep interior. These features include the transition between the crust and mantle, the subduction, sinking and deposition of slabs, upper mantle seismic anisotropy and its connection with plate motion, the position and extent of hotspots, small-scale heterogeneities in the mantle, the structure near the core–mantle boundary (CMB), anisotropy and rotation of the inner core. Resolving these features will require more and better data, and improved inversion and forward modeling algorithms for global 3-D Earth models with a broad wavenumber spectrum.

Verification of seismic modeling algorithms for 3-D models is difficult, because — unlike for the spherically symmetric case — in general, no analytical solutions exist which can be used as reference solutions (the recent work by Pollitz, 1998 is an exception). The comparison of synthetic seismograms computed with different numerical techniques is one of the most promising approaches for performing verification. Since the importance of full wave 3-D modeling will certainly grow, we propose that in addition to developing global 3-D reference Earth models, libraries of verified synthetic reference seismograms for particular source–receiver geometries should also be developed. This will enable modeling (and inversion) algorithms to be tested and their accuracy evaluated.

At the time when the COmparison of global SYnthetic seismogram techniques (COSY) workshop was held (IASPEI Meeting 1997), no global 3-D reference Earth model was available. Instead, the 3-D test model for the COSY Project was based on the temperature field obtained by 3-D mantle convection modeling. As we show below, this model has several features which a future 3-D reference model will probably share, in particular, the depth-dependence of the spectral properties as well as the amplitudes of the seismic velocity and density perturbations.

In the following sections, we present and discuss the 3-D model used in the simulations, review the seismic modeling algorithms, and discuss the modeling results for both the spherically symmetric background model and the 3-D model COSY01_50.

2. 3-D global test model

The COSY global 3-D test model is based on the spherically symmetric model, PREM (Dziewonski and Anderson, 1981), and a 3-D perturbation to this background defined between the Earth's surface and the CMB. Details on the background model are given in Section 4.1. The global test model was chosen so that its general characteristics, such as the amplitudes and the spectral properties of the perturbation in seismic velocity and density, are similar to results from global seismic tomography and geodynamics. We deliberately did not use one of the current global tomographic models, but rather chose an independent 3-D model based on the temperature field based on numerical simulation of mantle convection.

The convection simulations are described by Bunge et al. (1996; 1997). They investigated the effects of depth-dependent viscosity, heating mode (internal and from below), and an endothermic phase change in the upper mantle. For convection models with internal as well as bottom heating and a strong increase in viscosity in the lower mantle, the resulting temperature field had characteristics similar to the 3-D velocity perturbations of current tomographic models. In particular, layered viscosity led to long linear downwellings, similar to long quasi-lin-

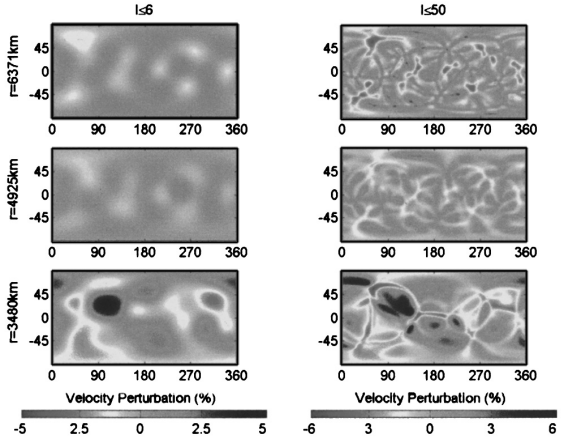

Fig. 1. COSY01_50 model perturbation on spherical shells at different depths. Left column: for harmonic degree $l \leq 6$. Right column: for harmonic degree $l \leq 50$. The perturbation (as a percentage) applies to the shear-wave velocity. P-wave velocity and density perturbations are half the shear-wave perturbation.

ear subduction zones penetrating into the mantle and, more importantly, to the presence of dominantly long-wavelength features in the lower mantle. These features are a consequence of the slow sinking of subducting lithosphere in the lower mantle because of the increase in viscosity with depth and are compatible with the results of Su and Dziewonski (1991).

The particular model we use stems from a simulation with internal heating and depth-dependent viscosity (and no phase changes in the upper mantle) described by Bunge et al. (1996). The 3-D temperature field is defined at 64 depth levels between the Earth's surface and the CMB and is represented in terms of spherical harmonic coefficients up to harmonic degree $l \leq 50$ using the following normalization (Stacey, 1992):

$$p_l^m(\cos\theta) = \left[(2-\delta_{m,0})(2l+1)\frac{(l-m)!}{(l+m)!}\right]^{1/2} \times P_{lm}(\cos\theta), \quad (1)$$

which is defined so that the mean square over a spherical surface is unity.

The temperature field has been normalized to represent a percentage perturbation in either P-velocity, S-velocity, or density. The maximum perturbation is $\pm 6\%$ The RMS perturbations are — depending on the maximum harmonic order — 0.36% ($l \leq 6$), 0.76% ($l \leq 32$) and 0.78% ($l \leq 50$). Examples of the perturbation fields are shown in Figs. 1 and 2 for different maximum harmonic orders and regions of the model. In the depth sections shown in Fig. 1, we observe that for low orders, the maximum perturbations occur in the lower mantle. For higher orders, we see sheet-like structures at the surface as well as longer wavelength structures at the bottom of the mantle. In the mid-mantle, the perturbations are — as is consistent with recent results from seismic tomography — smaller than at the top and the bottom of the mantle. The strong long-wavelength perturbation at the base of the mantle, which can also be observed in the low-order cross-sections of Fig. 2, is due to the slow sinking of the lithosphere in connection with the increase of viscosity with depth.

The characteristics of the perturbation model are summarized in the spectral heterogeneity map (SHM) shown in Fig. 3. The normalized sum D_l of the squared spherical harmonic coefficients A_{lm} and B_{lm},

$$D_l = \sum_{m=0}^{l} \left(A_{lm}^2 + B_{lm}^2\right), \quad (2)$$

is plotted against harmonic order and depth. The SHM shows the presence of the strongest perturba-

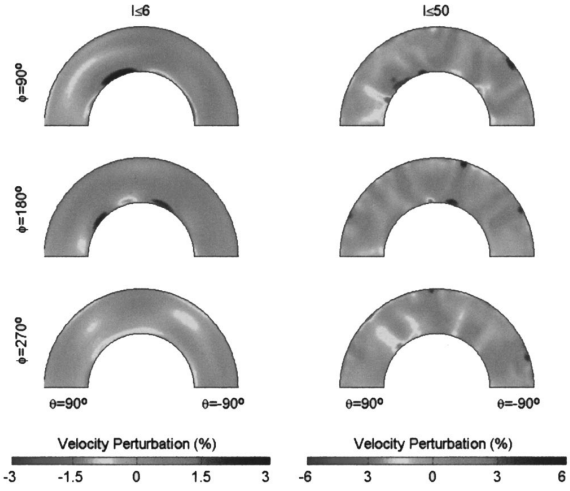

Fig. 2. COSY01_50 model perturbation in sections through the mantle at constant φ. The sections are shown in the planes through source and receiver locations in the numerical experiment. Left column: for harmonic degree $l \leq 6$. Right column: for harmonic degree $l \leq 50$.

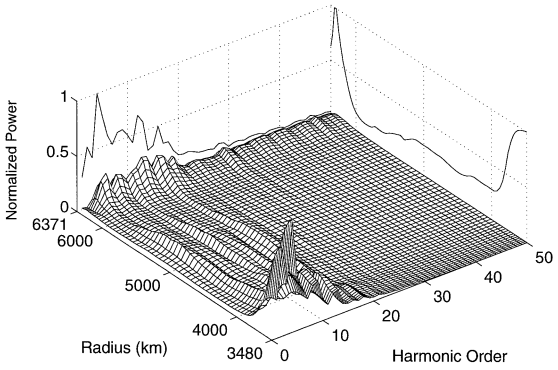

Fig. 3. SHM of the COSY01_50 model. Normalized power of the model perturbation is shown as a function of harmonic order and depth. Normalized sums over depth or harmonic order are projected to the boundaries. Note the higher-order perturbations near the surface and the dominant long-wavelength energy at the base of the mantle.

tions at low orders at the bottom of the mantle and the absence of strong short-wavelength features in this region. It also shows energy up to high orders at the top of the mantle which is due to the sheet-like structures seen in Figs. 1 and 2. Summing the power over all depth levels shows the characteristic dominance of long-wavelength features also observed by global tomography. Summing over all harmonic orders shows that lateral heterogeneity is strongest at the top and at the bottom of the mantle, which is also observed in the real Earth.

In this paper, synthetic seismograms for the model described in this section will be calculated using various techniques. Some of those techniques can only be applied to low-order models. It is clear that full wave effects will be most pronounced for models with energy at high harmonic orders and at high frequencies. It is envisaged that the spatial and temporal frequency range of test models and seismograms will be extended in the future as algorithms and computational hardware evolve.

3. Global synthetic seismogram methods

In this section, we briefly review global seismic modelling techniques with emphasis on the algorithms used in this study (see Table 1).

3.1. Review

The following review is by no means complete but should give some idea of the diversity of approaches for calculating seismograms in a spherical Earth. We focus on methods that allow computations of the complete wavefield. Therefore, ray-theoretical (and related) methods (e.g., Gilbert and Helmberger, 1972; Weber and Davis, 1990; Kendall and Thomson, 1993; Liu and Tromp, 1996) are not considered.

3.1.1. Spherically symmetric media

Most presently used methods for the calculation of 3-D seismograms are based upon a spherically symmetric model as a reference model for perturbation methods. Therefore, the calculation of seismograms for the spherically symmetric part of the model is still an essential ingredient for many forward calculations. Many calculations, including several in this paper, are based on the summation of normal modes (NM). The elastodynamic equations in spherical coordinates are transformed into the frequency domain and the displacement components are expanded in vector spherical harmonics (e.g., Alterman et al., 1959). The resulting system of differential equations for the expansion coefficients can be solved in many different ways. Gilbert (1980) solves numerically for the eigenfrequencies of the earth by an iterative procedure for the homogeneous system. This was extended to include point sources (Gilbert and Dziewonski, 1975) and combined with efficient algorithms to search for the eigenfrequencies (Woodhouse, 1988).

Other methods solve the inhomogeneous system of partial differential equations (including the source

Table 1
Annotation for the various algorithms used in the figures of this study

Abbreviations	Method	Author
NM1	Normal mode	Megnin
NM2	Normal mode	Clévédé
DSM1–3	Direct solution method; 1st, 2nd, 3rd-order Born	Takeuchi
GEM	Green's function evaluation	Dalkolmo
FD	Finite difference	Igel

term) directly in the frequency domain and synthetic seismograms are obtained after an inverse transform to the time domain (e.g., Chapman and Phinney, 1970; the WKBJ method used by Chapman and Orcutt, 1985; full wave theory used by Richards, 1973 and Choy, 1977). Alternatively, the reflectivity method (Fuchs, 1968), which was originally developed for horizontally layered media, was extended to spherical media (Fuchs and Müller, 1971; Müller, 1985) by use of an earth-flattening transformation. This transformation is exact for SH-waves (the toroidal problem), but it is not exact for P-SV wave propagation (the spheroidal problem). There are inaccuracies with this approach at low frequencies and for waves which turn near the center of the Earth (Choy et al., 1980).

An asymptotic approach to finding the eigenfrequencies and eigenfunctions of a spherical Earth model was presented by Zhao and Dahlen (1996), who applied conditions of constructive interference to body waves. Another approach for the calculation of global synthetic seismograms was introduced by Cummins et al. (1994a; b). They used the Direct Solution Method (DSM) developed by Geller and Ohminato (1994) and Geller and Takeuchi (1995) to solve the weak form of the wave equation (Galerkin formulation) similar to finite-element approaches. [2] An improved algorithm for the P-SV problem was presented by Takeuchi et al. (1996). Friederich and Dalkolmo (1995) used an alternative approach by numerically integrating the appropriate system of ordinary differential equations with source term and summation over vector spherical harmonics (see Takeuchi and Saito, 1972). An advantage of both this approach and the DSM approach is that neither eigenfrequencies nor eigenfunctions have to be evaluated in contrast to the large number of modes that have to be summed when the NM approach is used to compute complete seismograms.

Complete solutions to the general 3-D problem in a heterogeneous sphere still require impractically large amounts of CPU time if the finite-difference (FD) method is used. However, it is practical to obtain complete solutions to the wave equation for axi-symmetric media using the FD method. This approach — pioneered by Alterman et al. (1970) for P-SV wave propagation — allows the calculation of complete synthetic seismograms for spherically symmetric media for certain (axi-symmetric) source types. This approach was applied to long-period seismograms by Igel and Weber (1995; 1996) and Chaljub and Tarantola (1997).

3.1.2. Laterally heterogeneous media: perturbation methods

In present research, the calculation of synthetic seismograms is often undertaken by treating the 3-D part of the model as a slight perturbation to the spherically symmetric part of the Earth model. Such an approach is computationally much less demanding than calculating the complete wavefield for an arbitrary 3-D structure, but does not necessarily yield sufficient accuracy. Nevertheless, this approximate treatment of lateral heterogeneities has played a fundamental role in studies of the long-wavelength 3-D structure in the Earth's mantle. We will review only the key points of this approach here. The recent monograph by Dahlen and Tromp (1998) presents the various perturbation approaches for aspherical structures in detail.

The NM approach is most appropriate for long-period surface waves. Jordan (1978) and Woodhouse and Dziewonski (1984) used the great-circle approximation, assuming that seismograms are sensitive only to the horizontally averaged structure along a great-

[2] The 'weak form' and 'strong form' of partial differential equations (PDE) are standard terms in applied mathematics (see, e.g., Strang and Fix, 1973 or Geller and Ohminato, 1994), but appear not to be widely known in seismology. The strong form is the familiar form of the PDE. In the weak form, the solution is expanded in terms of trial functions (sometimes called coordinate functions), whose expansion coefficients become the unknown variables, and the PDE is thereby transformed into a set of algebraic equations (the weak form). The terms 'weak' and 'strong' denote the strictness of the conditions that must be satisfied by the respective solutions. Let us use the elastic equation of motion as an example. The weak form solutions need only explicitly satisfy continuity of displacement, as continuity of traction and free surface boundary conditions are 'natural' conditions that are automatically satisfied (at least in an approximate sense) by the weak form solutions. In contrast. the strong form solutions must explicitly satisfy continuity of traction and free surface boundary conditions, and are thus subject to 'stronger' requirements. Continuity of displacement is an 'essential' condition that must be explicitly satisfied by both the strong and weak form solutions, as must zero-displacement boundary conditions.

circle path between source and receiver. First-order perturbation theory for a slightly aspherical Earth in the time-domain was developed by Woodhouse (1983) and Tanimoto (1984). Further approximations to the first-order perturbation theory were introduced by Romanowicz and Roult (1986), Romanowicz (1987) using an asymptotic formalism, and Park (1987), and Dahlen (1987), introducing the sub-space projection method, and Mochizuki (1988), and Pollitz (1992).

Where the scale length of the lateral heterogeneity is much longer than the wavelength (of surface waves), generalized ray theory can be applied in combination with the Born approximation (e.g., Snieder, 1986, 1988; Snieder and Romanowicz, 1988; Romanowicz and Snieder, 1988). The studies by Mochizuki (1986), Park (1987) and Romanowicz (1987) showed that the path-average approximation (PAVA) commonly used in surface wave studies is equivalent to zero-order perturbation theory when coupling along branch is taken into account. Later, this approach was also applied to body waves (Woodhouse and Dziewonski, 1987; Tanimoto, 1990), but its validity is questionable for this case as the sensitivity of body waves to the (varying) structure along the ray path is not accounted for. Li and Tanimoto (1993) suggested that this drawback can be avoided by taking into account cross-branch modal coupling in an asymptotic fashion. This approach was extended by Li and Romanowicz (1995) who introduced the ''nonlinear asymptotic coupling theory'' (NACT), thereby avoiding restrictions as to the length of the synthetic seismograms. The effects of these various approximations on the resolution of tomographic images and particularly the superiority of the NACT approach over the PAVA approach were described by Li and Romanowicz (1995). Marquering and Snieder (1995) developed an equivalent method using a travelling wave approach. The effects of the Born approximation for slightly aspherical Earth structures was investigated by Cummins (1992). The scattering of surface waves using various approximations was studied by Friederich and Wielandt (1993). Tromp and Dahlen (1990) presented formulae for NM solutions based on the Born approximation which take into account higher order scattering terms by formal summation over the Born series.

Su et al. (1993) developed two approaches for aspherical structures for surface wave seismograms based on the Born approximation. They performed various tests and pointed out the importance of incorporating mode coupling. Takeuchi et al. (2000) extended the DSM method to compute complete synthetic seismograms for laterally heterogeneous media based on the first and higher-order Born approximation. Capdeville et al. (2000) used NM coupling to investigate 3-D effects on surface waves.

3.1.3. Laterally heterogeneous media: complete solutions

In the past decade, many methods have been developed for the calculation of wave propagation in 3-D heterogeneous media without using perturbation approximations. These efforts have been most successful for long-period surface waves because of the relatively light computational requirements. Variational (Galerkin) formulations of the problem of an aspherical anelastic Earth were applied by Park (1986), Park and Gilbert (1986), and Morris et al. (1987), although due to the computational costs these techniques are practical only at low frequencies. The Galerkin method was also applied to zonal (axi-symmetric) structures by Park and Yu (1992) and Yu and Park (1993). Lognonné and Romanowicz (1990) and Lognonné (1991) used high-order perturbation theory up to order n and showed that for all practical purposes order 3 was sufficient to achieve a degree of accuracy equivalent to the variational approach at low frequencies. Hara et al. (1993) used the DSM to compute long-period surface waves without perturbation approximations, and used this approach to invert iteratively for long-wavelength 3-D upper mantle S-velocities.

In contrast, due to the much greater computational requirements, methods for computing complete (including both body and surface waves) synthetics in 3-D models are much less advanced. Most of these techniques have been developed in a cartesian coordinate system. The reason is that the equations in spherical media are more complicated and regular grid methods such as the FD method or the pseudo-spectral method cannot be readily applied to a whole sphere unless a multi-domain approach is adopted (Thomas et al., 1999). Early attempts to solve the elastic wave equation in spherical coordinates explic-

itly by numerical methods (e.g., Alterman et al., 1970) were impractical because of the limitations of available computational facilities. With the advent of parallel supercomputing and the dawn of the TeraFlop era, the calculation of synthetic seismograms for a 3-D sphere with purely numerical techniques is becoming feasible. The first attempts to apply the FD method to realistic global wave propagation were carried out by Igel and Weber (1995; 1996) and Chaljub and Tarantola (1997). Their algorithms solved the wave equation in an axi-symmetric form, thereby reducing the problem to two dimensions. In the axi-symmetric form, the space-dependent fields in the governing equations are independent of longitude. Thus, the model, wavefield and source terms are all axi-symmetric, which limits the applicability of this approach to sources of toroidal and explosion type. With the use of parallel hardware, global wavefields with dominant periods of around 10 s can now be simulated following this approach. As these techniques allow the calculation of the complete wavefield, the effects of strong lateral heterogeneity such as that within subduction zones can be investigated.

Regular grid methods are inappropriate to model a complete sphere in a single-domain approach. Therefore, a multidomain approach was introduced for the SH case (Igel and Gudmundsson, 1997) and for the acoustic case (Thomas et al., 1999), allowing wavefield calculation in a full sphere for zonal models. A pseudo-spectral technique based on Chebyshev polynomials was introduced by Igel (1999) for spherical sections. This algorithm allows the study of azimuthal effects of 3-D structure such as subduction zones. A complete solution for spherical axi-symmetric media based on the DSM approach was presented by Cummins et al. (1997). The ultimate goal is to be able to calculate seismograms for an arbitrary 3-D sphere.

3.2. Algorithms used in this study

We summarize the various methods and algorithms used to compute synthetic seismograms presented in this paper (see Table 1).

3.2.1. NM summation (NM1,2)

The modal superposition technique used in this study is the path average approximation referred to as PAVA (Woodhouse and Dziewonski, 1984). In the PAVA approach, seismograms are calculated under the assumption that the horizontally averaged structure along the great-circle path between the source and the receiver governs the effects of lateral heterogeneity. This is equivalent to considering only the coupling of modes along a single dispersion branch and ignoring coupling between modes of different branches. A detailed comparison of PAVA and the more accurate nonlinear asymptotic coupling (NACT) approach by Li and Tanimoto (1993) was carried out by Li and Romanowicz (1995). The improvement of NACT over PAVA is mainly significant for body waves. For the COSY 3-D test model, only PAVA seismograms were available (Megnin, NM1). Further NM seismograms were submitted (Clévédé, NM2) for the spherically symmetric PREM model. As some of the subroutines for calculating the NM eigensolutions are the same in both of these algorithms (NM1,2), their results should not be considered entirely independent.

3.2.2. GEMINI (GEM)

This method, developed by Friederich and Dalkolmo (1995) for spherically symmetric media, uses neither modal superposition nor an earth-flattening transformation. The strong form of the system of ordinary partial differential equations including the source terms (Takeuchi and Saito, 1972) is numerically integrated and summed over vector spherical harmonics. As the solutions are evaluated in the discrete frequency domain, the numerical effort is proportional to the length of the desired seismograms for a fixed frequency band. This method requires less computational effort than NM techniques for higher frequency applications. In this approach, the expansion coefficients of the spherical harmonics are directly evaluated using second-order minors. The material parameters between discontinuities are represented by continuous functions, so there is no need for subdivision into homogeneous shells as is the case for the reflectivity technique. The synthetic seismograms are obtained after direct summation over the vector spherical harmonics and numerical inverse Fourier transform. Temporal aliasing is avoided by evaluating the Green's function at complex frequencies (Phinney, 1965).

3.2.3. DSM1–3

The DSM was first presented by Hara et al. (1991), who used the eigenfunctions of degenerate singlets of a spherically symmetric model as trial functions. The general DSM formulation was presented by Geller and Ohminato (1994). The DSM allows the computation of synthetic seismograms and their partial derivatives by solving the weak form of the elastic wave equation. It transforms the weak form into a system of linear equations, which is constructed using trial functions. In the spherically symmetric case, no approximations are made and the complete wavefield is simulated. Cummins et al. (1994a; b) applied this method to spherically symmetricmedia (SH and P-SV cases). Later, this approach was extended to rotationally symmetric media (Cummins et al., 1997) using the optimally accurate numerical operators derived by Geller and Takeuchi (1995). The DSM synthetics presented in this paper are based on an extension of the DSM method to 3-D media using the first-order and/or higher-order Born approximation (Takeuchi et al., 2000). The operators used in the DSM can also be transformed and applied in explicit time-domain algorithms such as the FD method using purely local trial functions (Geller and Takeuchi, 1998; Takeuchi and Geller, 2000).

3.2.4. FD

The wave equation can be solved numerically by replacing the partial differential equations with FD. All space-dependent fields are defined on regular grids. In spherical coordinates, this leads to space-dependent grid spacing. Because the stability of FD algorithms is proportional to the inverse of $\mathrm{d}x_j$, the increment along coordinate j, FD methods become impractible for whole Earth models in spherical coordinates. Nevertheless, they can be applied to the rotationally symmetric case, where the difficulties due to the grid spacing near the poles vanish and the depth range is restricted to a maximum depth to be adjusted for each particular problem. Igel and Gudmundsson (1997), Igel and Weber (1995; 1996) and Thomas et al. (1999) developed algorithms for the SH-, P-SV and acoustic cases for rotationally symmetric Earth models. Although the restriction to rotationally symmetric models seems severe, many model-dependent wave propagation phenomena can be studied for short length-scale models and high frequencies.

4. Computational results: spherically symmetric model

In this section, we will compare synthetic seismograms for the spherically symmetric background model used below in the 3-D study. The verification of the accuracy of the synthetics for this case is essential before we can consider 3-D models. For the dislocation source type (strike–slip) and receiver locations considered here (Fig. 4), only transverse displacement will be considered, and for the case of an explosive source, only P-SV motion will be considered. The seismic wavefield velocities rather than displacements are computed and are recorded at the Earth's surface at the receiver locations given in Fig. 4.

For reasons of symmetry, it is sufficient to consider only three of the five receiver locations (namely, receivers 1–3 Fig. 4). The algorithms compared are listed in Table 1. The ''author'' column in this table indicates which author of the present paper was primarily responsible for computing the synthetics using the method shown, rather than the authorship of the software used. In some cases, both are identical, but in others, pre-existing software was used.

4.1. Model and simulation parameters

The spherically symmetric model used in this study is a slightly modified version of PREM. The original PREM model contains an ocean layer. In this study this layer was omitted and the parameters of the topmost crustal layer extended to a radius of 6371 km. The elastic parameters are the isotropic part of PREM without attenuation. Gravitational effects and the Earth's rotation are not taken into account.

The sources used in this study are located at a latitude of 90° (North Pole) at a depth of 100 km. Only two source types were used: (1) a strike–slip source $M_{xy} = M_{yx} = M_0$, all other $M_{ij} = 0$; and (2) an explosion source $M_{xx} = M_{yy} = M_{zz} = M_0$. In both cases, $M_0 = 10^{25}$ dyn cm. The seismograms were either submitted filtered (NM1, NM2) or as Green's functions (others) and filtered accordingly.

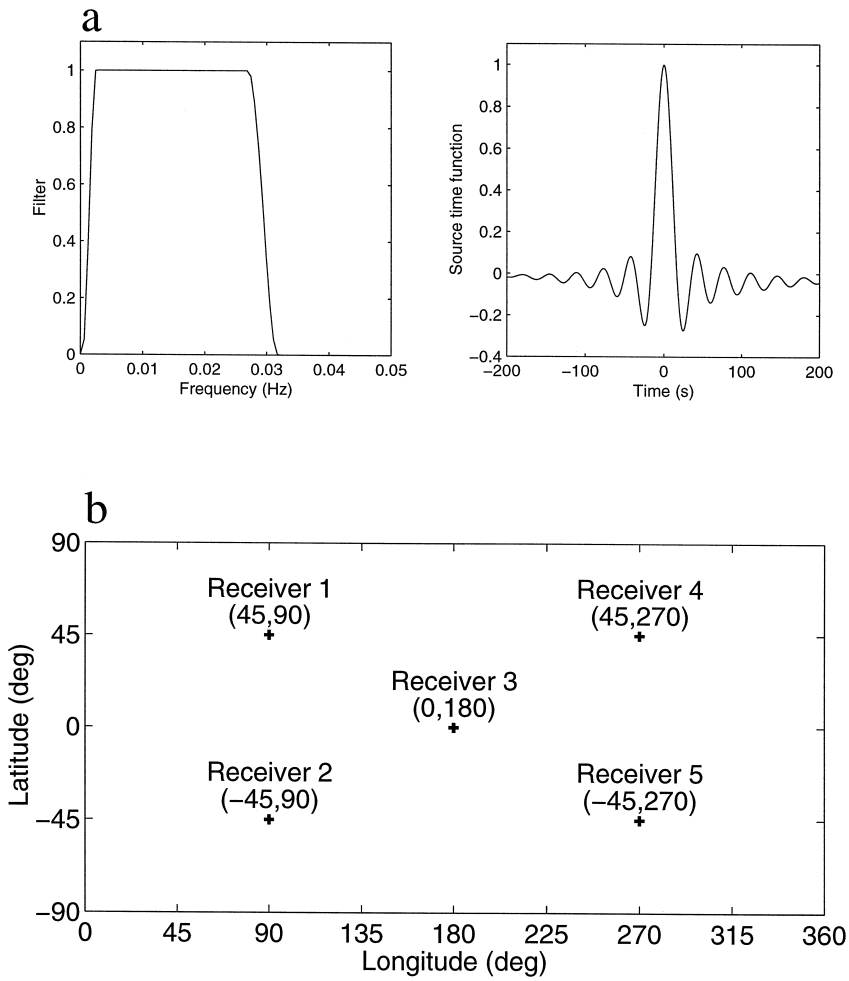

Fig. 4. (a) Left: Source spectrum used in the seismogram comparison. The spectrum is a cosine taper with corners at 31.4, 37.0, 400 and 3500 s period. Right: Spike filtered with the spectrum on the left. (b) Receiver locations (+) at the Earth's surface. In all our simulations, the epicenter is located at the North Pole (90° latitude), and the source depth is 100 km.

The spectrum of the filter and a filtered spike are shown in Fig. 4, top. The cosine-tapered filter has the form

$$F(\omega) = 0 \qquad \omega < \omega_1$$

$$F(\omega) = \frac{1}{2}\left(1 - \cos\left(\pi \frac{\omega - \omega_1}{\omega_2 - \omega_1}\right)\right) \qquad \omega_1 \le \omega < \omega_2$$

$$F(\omega) = 1 \qquad \omega_2 \le \omega < \omega_3$$

$$F(\omega) = \frac{1}{2}\left(1 + \cos\left(\pi \frac{\omega - \omega_3}{\omega_4 - \omega_3}\right)\right) \qquad \omega_3 \le \omega < \omega_4$$

$$F(\omega) = 0 \qquad \omega \ge \omega_4.$$

The corner frequencies ω_{1-4} are: $\omega_1 = 1/31.4\ \mathrm{s}^{-1}$; $\omega_2 = 1/37\ \mathrm{s}^{-1}$; $\omega_3 = 1/400\ \mathrm{s}^{-1}$; and $\omega_4 = 1/3500\ \mathrm{s}^{-1}$. This filter is used in all examples unless the seismograms are compared as a function of frequency (Figs. 7, 9, 12 and 14). In the other cases, the Green's functions were convolved with a source time function of the form

$$s(t) = -2\alpha t e^{\alpha^2 t^2}$$

where t is time and $\alpha = 4/T$, T being the dominant period.

4.2. Strike–slip source — SH motion

Seismograms for a receiver at an epicentral distance of 45° from a strike–slip source are shown in Fig. 5 (top). The wavefields were filtered so that a dominant period of 50 s was obtained. We show both the individual traces (left) as well as the difference between each of the traces and one of the NM solutions (NM1). To calculate the differences the seismograms were resampled with a sampling interval of 4 s. All of the seismograms are in good agreement before the arrival of the surface waves.

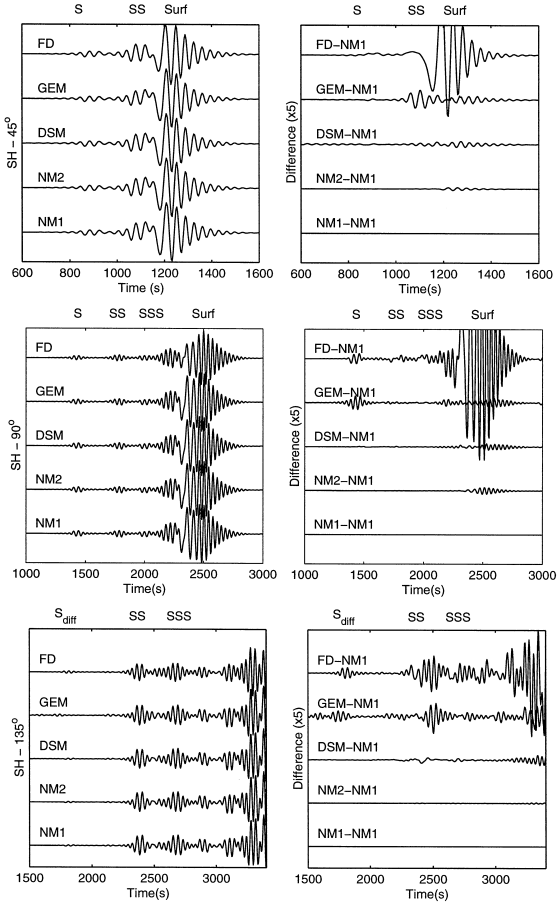

Fig. 5. Transverse component of displacement for a strike–slip source. Both seismograms (left column) and differences (with respect to NM1, right column, multiplied by a factor 5) are shown. Trace annotations are described in Table 1. The dominant period is 50 s. Top: epicentral distance 45°, middle: 90°, bottom: 135°. Some dominant phases are marked.

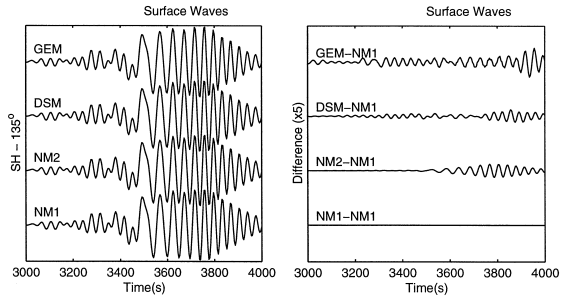

Fig. 6. Transverse component of displacement and the difference (multiplied by a factor 5) to NM1 for a strike–slip source observed at 135° epicentral distance (surface waves). Same parameters as previous figure.

The (quasi-) analytical [3] methods agree well for the surface wave arrivals. However, the FD solution is inaccurate in both amplitude and phase, although the envelope of the surface wave train is in overall agreement. The misfit observed in the differential seismogram is mainly due to a phase error in the FD solution. This is discussed in more detail below.

In Fig. 5 (middle), seismograms at an epicentral distance of 90° are shown. In general, the above discussion holds. The body waves are well modeled by all methods as is the qualitative behaviour of the surface wave train. The phase error of the FD surface wave solutions has increased, leading to a considerable misfit. At a distance of 135°, the solution for the body waves are still well modeled by all methods (Fig. 5, bottom), and all methods except FD are almost identical for the surface waves (Fig. 6).

The relative difference (root-mean square) of the energy in the seismograms for particular time win-

[3] Quasi-analytic denotes solutions of the equation of motion that are expressed partly but not entirely in terms of analytic basis functions. For problem in spherical coordinates, the θ- and ϕ-dependence of quasi-analytic basis functions is given by (vector)-spherical harmonics. For NM solutions, the vertical dependence of the basis functions is given by the eigenfunctions of the laterally homogeneous part of the model, which are determined numerically (see, e.g., Takeuchi and Saito, 1972). For the DSM implementation used in this paper, the vertical dependence of the basis functions is purely local (i.e., essentially the same as used in local finite element or FD calculations). In contrast, purely numerical methods such as FD use local basis functions for both the vertical and horizontal dependence of the solution.

dows is shown in Table 2 for an epicentral distance of 45°. The choice of NM1 as a reference solution is arbitrary. The results for the body wave time window shows that all methods are identical within 0.5%. The results for the surface waves confirm the problems of the FD solution for surface waves. The level of accuracy for all other techniques is basically the same for body and surface waves.

We now investigate whether the accuracy depends on epicentral distance. Accumulation of errors is expected for FD as distance increases, but not for the other methods, as they are all Fourier (spherical harmonic) methods. Table 3 shows the difference of the DSM and FD solutions and the NM solutions (NM1) as a function of epicentral distance for a time window containing the body wave arrivals. We can see — as expected — that the FD solutions are decreasingly accurate with increasing distance.

A further point of interest is the convergence of numerical solutions, when the effective sampling of the wavefield is increased (i.e., when the frequency is decreased without changing the grid spacing). In Fig. 7, part of the seismograms at 45° distance are convolved with source wavelets of increasing dominant period. This effectively increases the number of grid points per wavelength with which the wavefield is sampled. The time window contains the arrivals of the *S* and *sS* phases. We compare the GEM, DSM and FD solutions for which impulse responses were available. The solutions diverge for dominant periods smaller than 15 s as the particular algorithms were not run with grids that support those high frequencies with sufficient accuracy. However, DSM and FD both have coherent high-frequency energy, which are probably actual phases (e.g., before and after *sS*).

Table 2
Relative difference (as a percentage) between the SH seismograms for an epicentral distance of 45°. The upper right triangle shows the difference for the body waves (700 s $\leq t \leq$ 1000 s) and the lower left triangle shows the difference in a time window containing the surface waves (1100 s $\leq t \leq$ 1500 s)

Δ (%)	NM1	NM2	DSM	GEM	FD
NM1		0.0009	0.42	0.36	0.16
NM2	0.009		0.42	0.37	0.15
DSM	0.05	0.08		0.37	0.43
GEM	0.31	0.33	0.18		0.21
FD	9.3	9.6	8.9	9.1	

Table 3
Relative difference (as a percentage) between the SH seismograms as a function of epicentral distance in a window containing the body wave arrivals

Δ (%)	45°	90°	135°
FD–NM	0.16	0.9	2.1
DSM–NM	0.42	0.10	0.19

The waveforms are very similar for periods $\geq$ 20 s. The difference between FD and DSM rapidly drops below 0.5% for periods $\geq$ 20 s, indicating that the solutions have converged. The differences with GEM converge more slowly, indicating some slight differences in either the model or source term.

4.3. Explosion source — P-SV motion

The results for the same receiver locations for an explosion source are shown in Fig. 8. The vertical component of velocity is shown. At an epicentral distance of 45°, the body waves are well modeled by all techniques, but there are some differences in the amplitude of the surface waves. As in the SH case, FD does not accurately model the surface wave train. At larger epicentral distances (90° and 135°), the

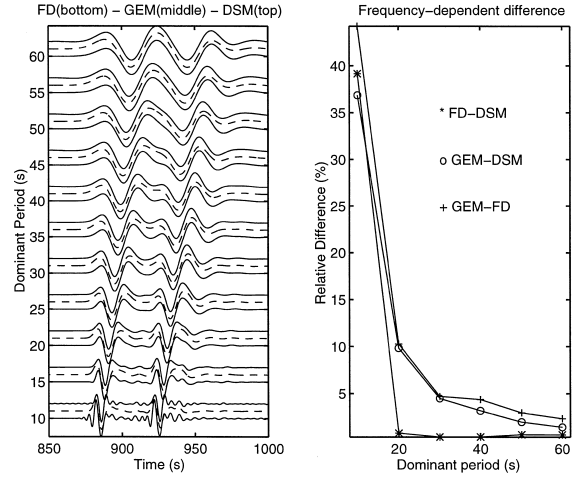

Fig. 7. Frequency-dependence of difference between FD, GEM and DSM solutions for a time window containing the *S* and *sS* arrivals at 45° epicentral distance. Left: The Green's functions convolved with source wavelets of various dominant periods. Right: Difference (as a percentage) between the various methods as a function of dominant period.

body wave arrivals for all the methods (FD excluded) match well, apart from small deviations in amplitude and some low-frequency energy of unknown origin, despite the complexity of the seismograms.

The relative differences (as a percentage) are shown in Table 4 for both body and surface waves at 45°. The two NM approaches are basically identical with GEM and DSM having small differences in some of the later body wave arrivals and also some differences in the surface waveform. The FD solution has an average misfit of around 5% for the body waves and 30% for the surface waves.

The frequency-dependence of the difference is studied in Fig. 9 for receiver 1 at 45 for a window containing the arrivals of the *P* and *PP* phases. The RMS-difference between the DSM and GEM solutions becomes smaller with increasing dominant period. However, the FD solution has a slightly different relative amplitude of the *P* and *PP* phases, which can be seen in Fig. 8 (top). This relative difference seems to be more significant at longer dominant periods which leads to the increasing misfit with dominant period.

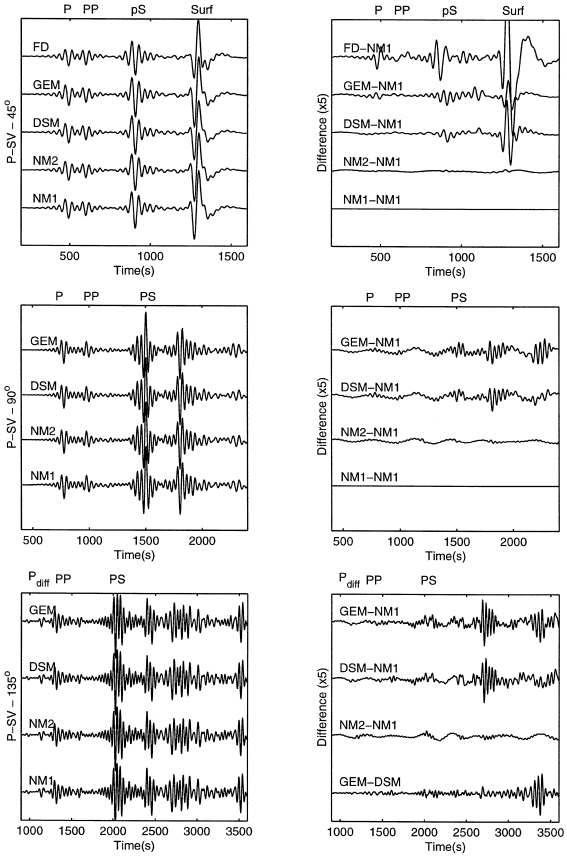

Fig. 8. Vertical component of displacement and the differences (multiplied by a factor 5) for an explosion source at 90° latitude. Trace annotations are described in Table 1. The dominant period is 50 s. Top: epicentral distance 45°. Middle: 90°. Bottom: 135°. Same amplitude scaling for all traces.

Table 4
Relative difference (as a percentage) between the P-SV seismograms for an epicentral distance of 45°. The upper right triangle shows the difference for the body waves (200 s $\leq t \leq$ 1100 s) and the lower left triangle shows differences for the surface waves (1100 s $\leq t \leq$ 1600 s)

Δ (%)	NM1	NM2	DSM	GEM	FD
NM1		0.068	0.45	0.81	5.6
NM2	0.042		0.49	0.87	5.7
DSM	1.90	2.08		0.48	5.2
GEM	1.00	1.13	0.99		4.9
FD	29.5	29.3	22.9	23.2	

5. Results: COSY01_50 model

In this section, we compare seismograms calculated for the COSY01_50 model for various maximum harmonic order of the 3-D model perturbation. Waveform synthetic data for the 3-D model were only available for the strike–slip source, and we therefore compare only synthetics for the transverse components. The methods available for the 3-D study were the NM approach using the PAVA (NM1), the DSM approach using the Born approximation of various orders (DSM1–3, see Takeuchi et al., 2000 for details), and the axi-symmetric FD approach. The main limitation at present is the frequency range that can be attained with these techniques using currently available computational facilities. The bulk of the comparative figures were obtained using a filter with a dominant period of around 50 s.

Waveforms of the transverse motion for the COSY01_50 model with harmonic order $l \leq 6$ as well as seismograms for the spherically symmetric model PREM are shown in Fig. 10. The seismograms for the perturbed and unperturbed Earth mod-

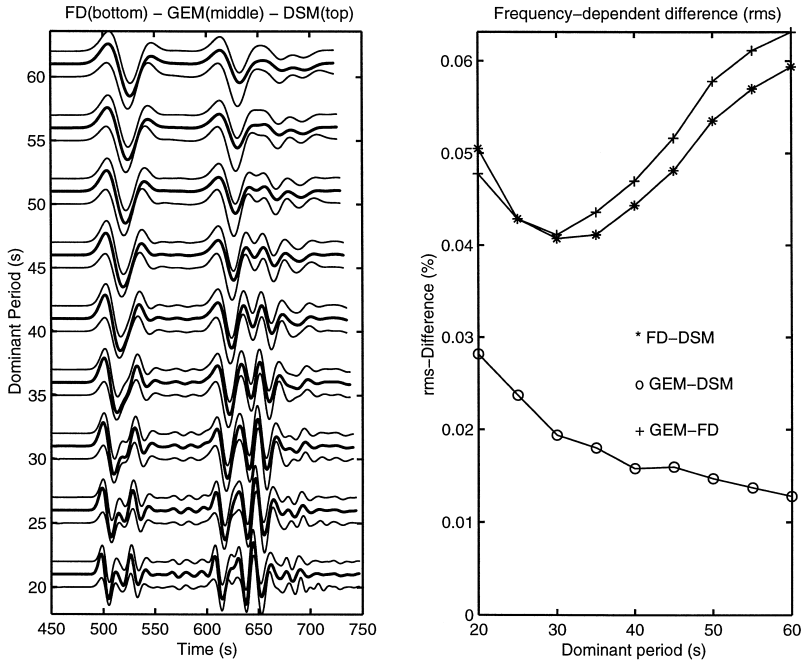

Fig. 9. Frequency-dependent difference between FD, GEM and DSM solutions for a time window containing the *P* and *PP* arrivals at 45° epicentral distance. Left: The Green's functions convolved with source wavelets of various dominant period. Right: Difference (as a percentage) as a function of dominant period.

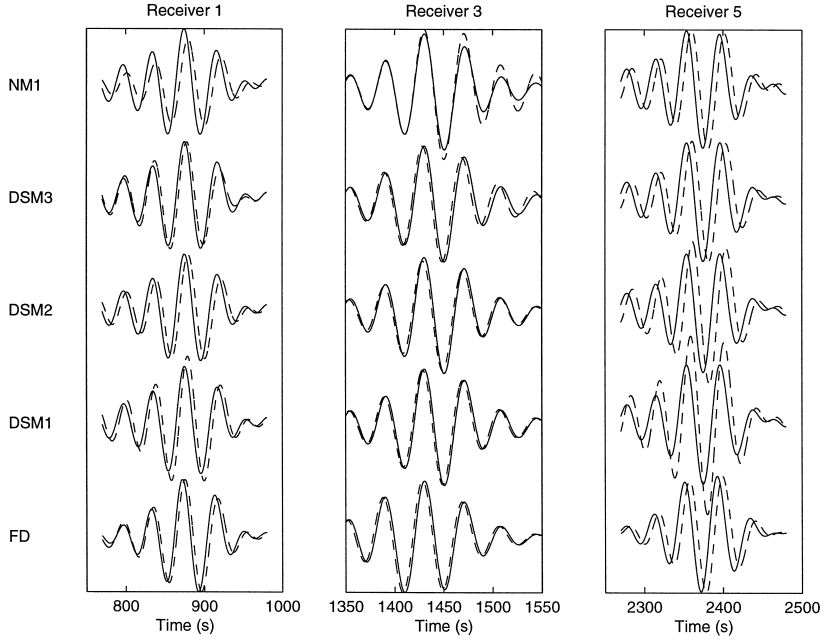

Fig. 10. Comparison of waveforms (transverse displacement) for *S* (receiver 1), *SS* (receivers 3 and 5) for PREM (solid) and COSY01_50 (dashed) with maximum harmonic order 6. Note the improving amplitude characteristics with increasing order of the Born approximation for the DSM seismograms.

Table 5
Comparison of traveltime perturbations obtained from the synthetic seismograms with ray-theory (R-Th). The traveltime perturbations due to the COSY01_50 3-D model perturbation were determined by cross-correlating the corresponding seismogram window with the one obtained for the PREM model

ΔT (s)	FD	DSM1	DSM2	DSM3	NM1	R-Th
S (45°)	3.9	4.0	4.9	4.2	5.1	4.3
SS (90°)	−2.0	−1.6	−1.6	−1.6	−0.5	−2.8
SS (135°)	6.6	4.8	7.0	6.8	6.5	6.0

els are superimposed to highlight the differential effects. The time window contains the *S* (receiver 1) or *SS* (receiver 3 and 5) arrivals. In order to compare the differential effects due to the 3-D structure, the traveltime perturbation of the wavegroup in this time window is extracted by cross-correlating the seismograms for the spherically symmetric PREM model and the traces for the 3-D model. As the seismograms were resampled to a sampling rate of 10 Hz, the error of the traveltime perturbation should be O(0.1 s). The PREM and 3-D seismograms are shown with correct relative amplitudes. The traveltime perturbations for the various techniques are summarized in Table 5 and compared with results from ray-theory. Full ray-tracing for 3-D heterogeneous models was undertaken. Takeuchi et al. (2000) showed that assuming ray-path perturbation as second-order perturbation is a good approximation for the low-degree COSY model. While all methods agree on the sign of the traveltime perturbations, there is considerable scatter in the magnitude of these effects.

The seismograms in Fig. 10 show a considerable difference between the various methods as far as the amplitudes are concerned. Apart from the FD and DSM3 solutions, there are significant differences in the amplitudes of the synthetics for the spherically symmetric and laterally heterogeneous models for an epicentral distance of 135° (receiver 5). The DSM1 solution shows an increase in amplitude, which seems to be proportional to the traveltime perturbation (and thus the velocity anomaly encountered along the raypath). This amplitude effect vanishes when third-order terms are included (DSM3). The amplitude effects seen in the NM1 solution do not seem to

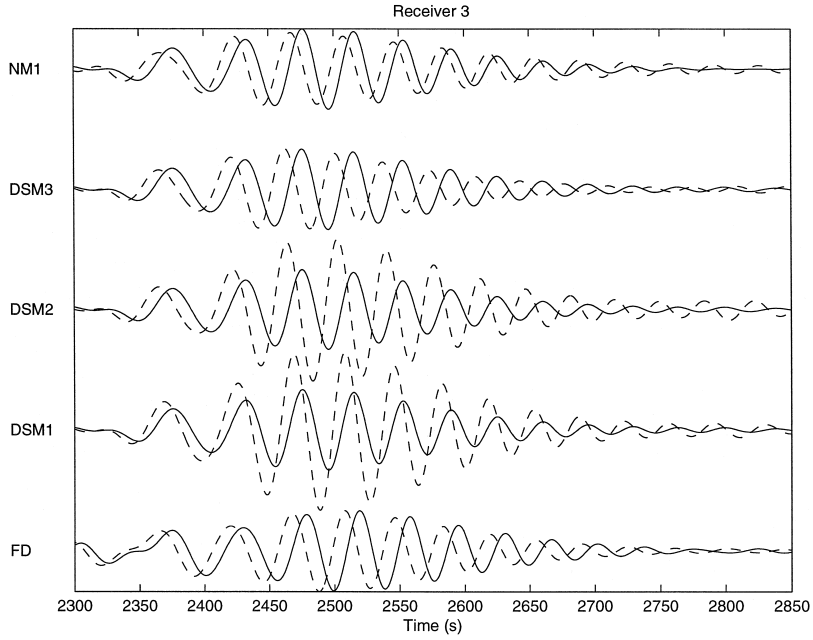

Fig. 11. Comparison of waveforms (transverse displacement) for surface waves at an epicentral distance of 90° for PREM (solid) and COSY01_50 (dashed) with maximum harmonic order 6. Note the improving amplitude characteristics with increasing order of the Born approximation for the DSM seismograms.

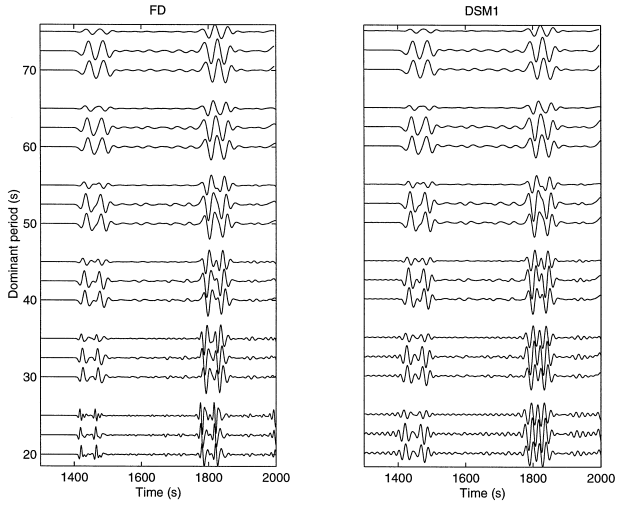

Fig. 12. Comparison of waveforms at an epicentral distance of 90° for PREM and COSY01_50 with maximum harmonic order 6 as a function of dominant period. The seismogram groups are for PREM (bottom), COSY (middle) and the residuals (top). The time window contains the arrivals of *S*, *sS*, *SS* and *sSS*.

show this correlation. However, it is well known (e.g., Li and Romanowicz, 1995) that the PAVA approximation performs badly for body waves.

The amplitude effects are even more pronounced in the surface wave trains shown in Fig. 11. The DSM1 surface wave amplitudes are increased by almost 30%. Although — as observed above — there is a static phase error in the FD solution for the surface waves, it is likely that the differential effects are correctly modeled. The FD solution does not show such an amplitude increase nor does the DSM3 solution or — in this case — the NM1 solution. These amplitude effects are discussed in more detail below.

For the DSM and FD approaches, the Green's functions were available, which allows us to investigate the frequency-dependent behaviour of the 3-D solutions (Fig. 12). The chosen time window contains the arrivals of *S*, *sS*, *SS* and *sSS* phases. The Green's functions are convolved with wavelets of varying dominant period. The differential seismograms for the DSM1 and FD solutions agree well for dominant periods ≥ 40 s.

Seismograms for models up to harmonic degree 50 were only available for the axi-symmetric FD approach and the NM methods. Seismograms for an epicentral distance of 135° containing the *SS* and *SSS* wavetrains for various models are shown in Fig. 13. For the low-order model ($l \leq 6$), the differential effects are very similar in amplitude and travel time. The maximum amplitude of the traveltime perturbations increases with increasing harmonic order (see Figs. 1 and 2). For the model with perturbations up to $l = 50$, the traveltime perturbations of the FD

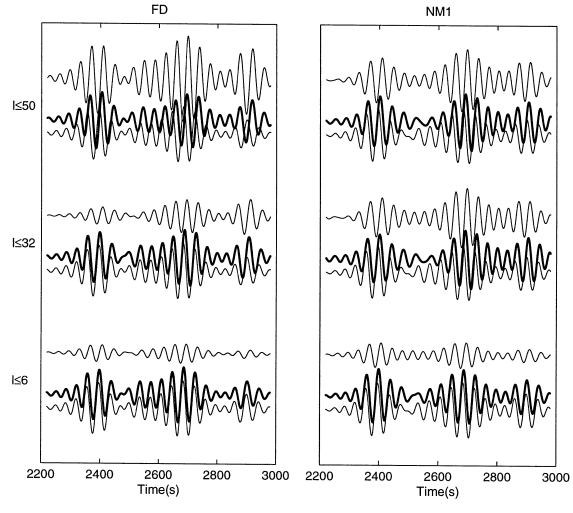

Fig. 13. Comparison of waveforms for models with different maximum harmonic order. Seismograms for receiver 2 (epicentral distance 135°) are shown. The seismogram groups are for PREM (bottom), COSY (middle, thick line) and the residuals (top). Left column: FD solutions. Right column: NM1 solutions.

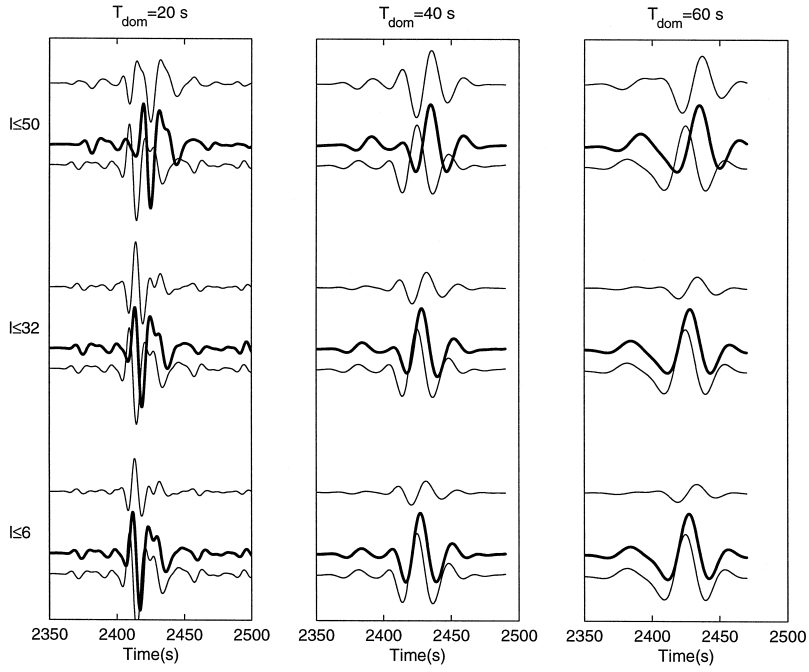

Fig. 14. FD seismograms for models with different maximum harmonic order at various dominant periods. Seismograms for receiver 2 (epicentral distance 135°) are shown. The seismogram groups are for PREM (bottom), COSY (middle, thick line) and the residuals (top, multiplied by a factor of 1/2).

solutions are considerably larger than those from the NM solutions. This may indicate that we are outside the domain of applicability of the path-average perturbation approach and that its solutions are no longer accurate.

The effects of both dominant period and maximum harmonic order in the model perturbation are illustrated in Fig. 14 for an epicentral distance of 135° and a time window containing the *SS* arrival. For the frequency range and the model wavenumber range considered, the waveform effects are small. The 3-D model perturbation predominantly affects the arrival time of the individual phases.

6. Discussion

It is fair to say that the calculation of complete synthetic seismograms for 3-D models on a planetary scale is still in its infancy. The reasons are manifold. Historically, the calculation of long-period synthetic seismograms for spherical Earth models was predominantly built around the NM approach. As in many cases, it is appropriate to view the Earth as spherically symmetric to first order, the calculation of complete waveforms for spherically symmetric Earth models has been one of the most powerful tools in global seismology. Due to the — almost — spherical shape of our planet, it is natural that the first waveform algorithms for 3-D media were based on the NM approach, and combined with perturbation theory to account for ''small'' perturbations thereto. The limitations of this approach in the context of scattering were equivalent to adopting a ray-theoretical ''ansatz'' for the perturbation of the spherically symmetric model. The early approaches were soon extended to higher orders. Nevertheless, an algorithm for complete 3-D seismograms at periods below 100 s for models with 3-D structure with harmonic order greater than $l = 50$ based on NM, which has to include complete intermodal coupling, does not seem to be in sight. This is due to the fact that the number of modes to couple grows rapidly with frequency.

The rapid development of purely numerical techniques for seismic wave propagation, particularly in the field of seismic exploration, has not been paralleled in global seismology. One of the reasons may be the difficulties of applying standard numerical techniques in 3-D spherical geometry. The accurate calculation of synthetic seismograms for a laterally and vertically heterogeneous spherical model poses formidable challenges concerning both the algorithmic approach and the computational effort. However, the ease with which the seismic wave equation can be parallelized on massively parallel supercomputers seems likely to make such algorithms feasible for global models in the near future.

6.1. Spherically symmetric models

In this context, a detailed look at how purely numerical solutions to the wave equation — even for spherically symmetric models — compare with other (e.g., quasi-analytic) approaches is important to determine the direction of future work on numerical algorithms. It is too early for an extensive look at complete 3-D solutions, as hardly any algorithms exist at present in production mode, as is highlighted through this study. Therefore, this study should be considered as preliminary in nature. Future studies with a more detailed investigation of 3-D algorithms, possibly at higher frequencies and model wavenumbers, are required.

Nevertheless, this study has shown several major trends. As expected, (after quite some iterations) the synthetic seismograms for the quasi-analytic methods (NM1,2; GEM, DSM) shown in Figs. 5–9 agree well for spherically symmetric models. Even though this is encouraging, there are still differences (in the third decimal place) for reasons we have not yet fully identified. This must be investigated. The numerical solutions based on the FD method agree well with the other solutions for the body-wave part of the seismograms. However, as far as the surface waves are concerned, only the envelope of the surface wave train is correctly modeled while the FD solution shows an increasing phase shift with epicentral distance (e.g., Fig. 5). This is probably due to the implementation of the free surface boundary condition, which is of lower order than the high-order differential operators acting inside the medium. This must also be improved.

As the FD solutions are based on the zonal wave equation, the source is not a pure strike–slip source as in the other solutions, but a toroidal ring-source input at a grid point close to the axis or rotational symmetry. Although the radiation pattern of this source is very close to the radiation pattern of a strike–slip source, the fact that it is a ring source will introduce slight alterations to the far-field waveform. The axi-symmetric approach — although limited in the model geometry — will remain an important approach because — due to the reduction to essentially a 2-D problem — much higher frequencies can be achieved than with complete 3-D solutions. It will be a challenge to develop an algorithm that allows general sources to be modeled with this approach (and not only axi-symmetric source like toroidal ring sources or explosions), so that this approach can be used for modeling real data.

One of the great challenges for computing solutions to the wave equation in the time domain will be to minimize numerical artifacts such as numerical dispersion that cause waveform and traveltime errors particularly for long propagation distances. The numerical solutions (FD) used in this paper were based on fairly standard operators used in exploration seismology. More accurate extrapolation operators for the global problem are possible and the paper by Takeuchi and Geller (2000) in this issue represents an important step in this direction, particularly if their approach can be extended to spherical coordinates.

6.2. COSY01_50

The 3-D model perturbation allowed us to compare the differential effects of the various approaches. While the polarity of the traveltime perturbations are the same for all approaches, their magnitudes vary (Fig. 10; Table 5) even for the low-order model (harmonic order $l \leq 6$), where the ray-theoretical conditions clearly are fulfilled in the frequency range considered. This should be cause for concern, as these differences are mapped into model perturbations by the algorithms used in tomographic studies. A quantification of such effects are discussed in Clévéde et al. (2000). There are noticeable

unphysical amplitude effects observed for the low-order approaches (the PAVA — NM1, and the first- and second-order Born approximations of the DSM solutions). These effects are most pronounced for the surface waves.

The extension to higher orders clearly seems to eliminate these artifacts (Figs. 10 and 11). Presumably, the third-order Born series for the DSM approach is the same as the third order perturbation for NM. The equivalence of the first-order DSM and modal perturbation was demonstrated by Geller et al. (1990a; b). Their work supports the view that there is no fundamental difference between modal superposition and other quasi-analytic approaches (e.g., GEM, DSM). This approach can be, but has not yet been extended to higher orders. One of the findings of this paper that will help in applying the DSM approach successfully to real data modeling is that the third-order approximation has to be adopted to avoid the numerical amplitude errors described above. This highlights the importance of the comparison of synthetics computed with different methods. Further discussions of the effects of including higher-order terms can be found in Lognonné and Romanowicz (1990) and Takeuchi et al. (2000).

The differential effects for models with various maximum harmonic order (Fig. 13) indicate that while for low-order models, the perturbation approach (NM1) and the FD solutions are comparable, they diverge for models with larger perturbation amplitude and shorter spatial wavelength. This may be due to the fact that the perturbation approach has been extended beyond its domain of applicability. However, the difference may also be caused by the axi-symmetric approximation of the FD solution, which considers only the model perturbation in the plane through source and receiver. Only with complete 3-D solution will we be able to determine the correct 3-D behavior.

For the FD solutions, impulse responses for all models were available. This allows the study of the synthetic solutions as a function of frequency and maximum harmonic order in the model perturbation (Fig. 14). In the frequency and wavenumber bands considered, the differential effects are predominantly on the traveltimes of individual phases. As the capability of algorithms evolves, and wavefields and models with higher frequencies and wavenumbers are simulated, this type of processing will be important so that the limits of the various approaches can be investigated.

7. Conclusions: lessons from COSY

As far as the calculation of synthetic seismograms for Earth models on a planetary scale are concerned, we are at a turning point. The first generation of global 3-D tomographic models were obtained using modeling approaches, which have more or less severe limitations concerning traveltime and amplitude effects. With the increasing resolution of global and regional tomographic studies, the correct simulation of the complete wavefield, including all scattering effects, has become a major goal in theoretical global seismology. Some of the most interesting geodynamical features, such as the subduction of plates, are characterized by relatively strong seismic velocity perturbations, which can only be fully understood with complete synthetic modeling techniques.

The problem with numerical approaches is that often, the verification of computational codes, particularly for 3-D models, is difficult, as no analytical solutions exist. To facilitate and, in some respect, standardize the verification of global synthetic modeling algorithms in the future, we have proposed a 3-D test model in the form of seismic velocity and density perturbations to a spherically symmetric model (PREM) expanded in spherical harmonic coefficients up to degree 50 for 64 layers in the Earth's mantle. This model and the results shown in this study are accessible through the worldwide web (http://www.geophysik.uni-muenchen.de/COSY). It is envisioned that when the first generation of 3-D reference Earth models are available they can also be used as test models for future comparisons of synthetics.

As this area of research is in its infancy, the results shown here should be considered as preliminary. Nevertheless, the following general observations hold: (1) Purely numerical solutions to the wave equation in spherical geometry are now capable of competing with other more classical approaches such as perturbation theory, as far as the forward calculation of synthetic seismograms are concerned. (2) The investigation of the differential

effects of the various approaches shows that considerable differences (e.g., traveltime effects) are observed. This should be borne in mind when imaging real data. (3) The optimization of the spatial and temporal operators for the wave equation in spherical geometry will play a major role in making numerical algorithms for global seismology computationally efficient and thus feasible for use in actual data inversion.

Acknowledgements

First, we would like to thank Colin Thomson and Bob Engdahl, who enabled the workshop to be held at the IASPEI97 Meeting in Greece. The idea for such a workshop originated during discussions one of the authors (HI) had with Phil Cummins, Valeri Korneev and Roland Gritto. Their comments, suggestions and early contributions were invaluable. We also thank Torsten Dahm, Ikuko Fuji, Brian Kennett, Philippe Lognonné, Fred Pollitz, Paul Richards, Adam Schultz and John Woodhouse for their contributions and suggestions. This research was partly supported by grant GR3/10086 of the National Environmental Research Council (HI) and also through the German Research Foundation (HI, Heisenberg Program). This research was also supported by a grant from the Japanese Ministry of Education, Science and Culture and Sports (No. 10640403). N.T. was supported by a JSPS Fellowship for Young Scientists. We would also like to thank Jeroen Tromp and Mike Kendall for critically reviewing this manuscript.

References

Alterman, Z., Aboudi, J., Karal, F.C., 1970. Pulse propagation in a laterally heterogeneous solid elastic sphere. Geophys. J. R. Astron. Soc. 21, 243–260.

Alterman, Z., Jarosch, H., Pekeris, C., 1959. Oscillations of the Earth. Proc. R. Soc. London, Ser. A 252, 80–95.

Bunge, H.P., Richards, M.A., Baumgardner, J.R., 1996. Effect of depth-dependent viscosity on the planform of mantle convection. Nature 379, 436–438.

Bunge, H.P., Richards, M.A., Baumgardner, J.R., 1997. A sensitivity study of three-dimensional spherical mantle convection at 10(8) Rayleigh number: effects of depth-dependent viscosity, heating mode, and an endothermic phase change. J. Geophys. Res. 102, 11991–12007.

Capdeville, Y., Stutzmann, E., Montagner, J.P., 2000. Effect of a plume on long-period surface waves computed with normal mode coupling. Phys. Earth Planet. Inter. 119, 54–71.

Chaljub, E., Tarantola, A., 1997. Sensitivity of SS precursors to topography on the upper-mantle 660-km discontinuity. Geophys. Res. Lett. 24, 2613–2616.

Chapman, C.H., Orcutt, J.A., 1985. The computation of body wave synthetic seismograms in laterally homogeneous media. Rev. Geophys. 23, 105–163.

Chapman, C.H., Phinney, R.A., 1970. Diffraction of P waves by the core and an inhomogeneous mantle. Geophys. J. R. Astron. Soc. 21, 185–202.

Choy, G.L., 1977. Theoretical seismograms of core phases generated by frequency-dependent full-wave theory and their interpretation. Geophys. J. R. Astron. Soc. 51, 275–311.

Choy, G.L., Cormier, V.F., Kind, R., Müller, G., Richards, P.G., 1980. A comparison of synthetic seismograms of core phases generated by the full wave theory and the reflectivity method. Geophys. J. R. Astron. Soc. 61, 21–39.

Clévéde, E., Megnin, C., Romanowicz, B., Lognonné, P., 2000. Seismic waveform modeling and surface wave tomography in a three-dimensional Earth: asymptotic and non-asymptotic approaches. Phys. Earth Planet. Inter. 119, 37–56.

Cummins, P.R., 1992. Seismic body waves in a 3-D, slightly aspherical Earth: I. Testing the Born approximation. Geophys. J. Int. 109, 391–410.

Cummins, P.R., Geller, R.J., Hatori, T., Takeuchi, N., 1994a. DSM complete synthetic seismograms: SH, spherically symmetric, case. Geophys. Res. Lett. 21, 533–536.

Cummins, P.R., Geller, T., Takeuchi, N., 1994b. DSM complete synthetic seismograms: P-SV, spherically symmetric, case. Geophys. Res. Lett. 21, 1663–1666.

Cummins, P.R., Takeuchi, N., Geller, R.J., 1997. Computation of complete synthetic seismograms for laterally heterogeneous models using the direct solution method. Geophys. J. Int. 130, 1–16.

Dahlen, F.A., 1987. Multiplet coupling and the calculation of long-period synthetic seismograms. Geophys. J. R. Astron. Soc. 58, 1–33.

Dahlen, F.A., Tromp, J., 1998. Theoretical Global Seismology. Princeton Univ. Press.

Dziewonski, A.M., Anderson, D.L., 1981. Preliminary reference Earth model. Phys. Earth Planet. Inter. 25, 297–356.

Friederich, W., Dalkolmo, J., 1995. Complete synthetic seismograms for a spherically symmetric earth by a numerical computation of the Green's function in the frequency domain. Geophys. J. Int. 122, 537–550.

Friederich, W., Wielandt, E., 1993. Multiple forward scattering of surface waves: comparison with an exact solution and Born single-scattering methods. Geophys. J. Int. 112, 264–275.

Fuchs, K., 1968. The reflection of spherical waves from transition zones with arbitrary depth-dependent elastic moduli and density. J. Phys. Earth 16, 27–41.

Fuchs, K., Müller, G., 1971. Computation of synthetic seismograms with the reflectivity method and comparison with observations. Geophys. J. R. Astron. Soc. 23, 417–433.

Geller, R.J., Hara, T., Tsuboi, S., 1990a. On the equivalence of

two methods for computing partial derivatives of seismic waveforms. Geophys. J. Int. 100, 155–158.

Geller, R.J., Hara, T., Tsuboi, S., 1990b. On the equivalence of two methods for computing partial derivatives of seismic waveforms: II. Laterally homogeneous initial model. Geophys. J. Int. 102, 499–502.

Geller, R.J., Ohminato, T., 1994. Computation of synthetic seismograms and their partial derivatives for heterogeneous media with arbitrary natural boundary conditions using the direct solution method. Geophys. J. Int. 116, 421–446.

Geller, R.J., Takeuchi, N., 1995. A new method for computing highly accurate DSM synthetic seismograms. Geophys. J. Int. 123, 449–470.

Geller, R.J., Takeuchi, N., 1998. Optimally accurate time domain finite difference scheme for the elastic wave equation: one-dimensional case. Geophys. J. Int. 135, 48–62.

Gilbert, F., 1980. Introduction to low-frequency seismology. Physics of the Earth's Interior. Proc. Int. School of Physics, ''Enrico Fermi'', North-Holland, Amsterdam, pp. 127–151.

Gilbert, F., Dziewonski, A.M., 1975. An application of normal mode theory to the retrieval of structural parameters and source mechanisms for seismic spectra. Philos. Trans. R. Soc. London, Ser. A 278, 187–269.

Gilbert, F., Helmberger, D.V., 1972. Generalized ray theory for a layered sphere. Geophys. J. R. Astron. Soc. 27, 57–80.

Hara, T., Tsuboi, S., Geller, R.J., 1991. Inversion for laterally heterogeneous earth structure using a laterally heterogeneous starting model: preliminary results. Geophys. J. Int. 104, 523–540.

Hara, T., Tsuboi, S., Geller, R.J., 1993. Inversion for laterally heterogeneous upper mantle S-wave velocity structure using iterative waveform inversion. Geophys. J. Int. 115, 667–698.

Igel, H., 1999. Modeling wave propagation in 3-D spherical sections by the Chebyshev spectral method. Geophys. J. Int. 136, 559–567.

Igel, H., Gudmundsson, O., 1997. Frequency-dependent effects on travel times and waveforms of long-period S and SS waves. Phys. Earth Planet. Inter. 104, 229–246.

Igel, H., Weber, M., 1995. SH-wave propagation in the whole mantle using high-order finite differences. Geophys. Res. Lett. 22, 731–734.

Igel, H., Weber, M., 1996. P-SV wave propagation in the Earth's mantle using finite-differences: application to heterogeneous lowermost mantle structure. Geophys. Res. Lett. 23, 415–418.

Jordan, T.H., 1978. A procedure for estimating lateral variations from low-frequency eigenspectra data. Geophys. J. R. Astron. Soc. 52, 441–455.

Kendall, J.M., Thomson, C.J., 1993. Maslov ray summation, pseudo-caustics, Lagrangian equivalence and transient seismic waveforms. Geophys. J. Int. 113, 186–214.

Li, X.-D., Romanowicz, B., 1995. Comparison of global waveform inversion with and without considering cross-branch modal coupling. Geophys. J. Int. 121, 695–709.

Li, X.-D., Tanimoto, T., 1993. Waveforms of long-period body waves in a slightly aspherical Earth model. Geophys. J. Int. 112, 92–102.

Liu, X.-F., Tromp, J., 1996. Uniformly valid body-wave ray theory. Geophys. J. Int. 127, 461–491.

Lognonné, P., 1991. Normal modes and seismograms in an anelastic rotating Earth. J. Geophys. Res. 96, 20309–20319.

Lognonné, P., Romanowicz, B., 1990. Modelling of coupled normal modes of the Earth: the spectral method. Geophys. J. Int. 102, 365–395.

Marquering, H., Snieder, R., 1995. Surface-wave mode coupling for efficient forward modelling and inversion of body-wave phases. Geophys. J. Int. 120, 186–208.

Mochizuki, E., 1986. Free oscillations and surface waves of an aspherical Earth. Geophys. Res. Lett. 13, 1478–1481.

Mochizuki, E., 1988. A simple method to calculate synthetic long-period incorporating first order asymptotics. J. Phys. Earth 36, 229–236.

Morris, S., Geller, R.J., Kawakatsu, H., Tsuboi, S., 1987. Variational free oscillation computations for three laterally heterogeneous Earth models. Phys. Earth Planet. Inter. 47, 288–318.

Müller, G., 1985. The reflectivity method: a tutorial. Geophys. J. R. Astron. Soc. 58, 153–174.

Park, J., 1986. Synthetic seismograms from coupled free oscillations: the effects of lateral structure and rotation. J. Geophys. Res. 91, 6441–6464.

Park, J., 1987. Asymptotic coupled-mode expressions for multiplet amplitude anomalies and frequency shifts on an aspherical Earth. Geophys. J. R. Astron. Soc. 90, 129–169.

Park, J., Gilbert, F., 1986. Coupled free oscillations of an apsherical, dissipative, rotating Earth: Galerkin theory. J. Geophys. Res. 91, 7241–7260.

Park, J., Yu, Y., 1992. Anisotropy and coupled free oscillations: simplified models and surface wave observations. Geophys. J. Int. 110, 401–420.

Phinney, R.A., 1965. Theoretical calculation of the spectrum of first arrivals in layered elastic media. J. Geophys. Res. 70, 5107–5123.

Pollitz, F., 1992. Propagation of surface waves on a laterally heterogeneous earth: asymptotic solution of the two-dimensional wave equation. Geophys. J. Int. 111, 67–78.

Pollitz, F., 1998. Scattering of spherical elastic waves from a small-volume spherical inclusion. Geophys. J. Int. 134, 390–408.

Richards, P.G., 1973. Calculation of body waves for caustics and tunneling core phases. Geophys. J. R. Astron. Soc. 35, 243–264.

Romanowicz, B., 1987. Multiplet–multiplet coupling due to lateral heterogeneity: asymptotic effects on the amplitude and frequency of the Earth's normal modes. Geophys. J. R. Astron. Soc. 90, 75–100.

Romanowicz, B., Roult, G., 1986. First order asymptotics for the eigenfrequencies of the Earth and application to the retrieval of large-scale lateral variations of structure. Geophys. J. R. Astron. Soc. 87, 209–240.

Romanowicz, B., Snieder, R., 1988. A new formalism for the effect of lateral heterogeneity on normal modes and surface waves: II. General anisotropic perturbation. Geophys. J. 93, 91–99.

Snieder, R., 1986. 3-D linearized scattering of surface waves for surface wave holography. Geophys. J. R. Astron. Soc. 84, 581–606.

Snieder, R., 1988. Large scale waveform inversion of surface

waves for lateral heterogeneity: 2. Application to surface waves in Europe and the Mediterranean. J. Geophys. Res. 93, 12067–12080.

Snieder, R., Romanowicz, B., 1988. A new formalism for the effect of lateral heterogeneity on normal modes and surface waves: I. Isotropic perturbations, perturbations of interfaces and gravitational perturbances. Geophys. J. 92, 207–222.

Stacey, F.D., 1992. Physics of the Earth, 3rd edn. Brookfield Press.

Strang, G., Fix, G.J., 1973. An Analysis of the Finite Element Method. Prentice-Hall, Englewood Cliffs, NJ.

Su, L., Park, J., Yu, Y., 1993. Born seismograms using coupled free oscillations: the effects of strong coupling and anisotropy. Geophys. J. Int. 115, 849–862.

Su, W.J., Dziewonski, A.M., 1991. Predominance of long-wavelength heterogeneity in the mantle. Nature 352, 121–126.

Takeuchi, N., Geller, R.J., 2000. Optimally accurate second order time-domain finite-difference scheme for computing synthetic seismograms in 2-D and 3-D media. Phys. Earth Planet. Inter. 119, 103–138.

Takeuchi, N., Geller, R.J., Cummins, P., 1996. Highly accurate P-SV complete synthetic seismograms using modified DSM operators. Geophys. Res. Lett. 23, 1175–1178.

Takeuchi, N., Geller, R.J., Cummins, P.R., 2000. Complete synthetic seismograms for 3-D heterogeneous Earth models computed using modified DSM operators and their applicability to inversion for Earth structure. Phys. Earth Planet. Inter. 119, 25–36.

Takeuchi, H., Saito, M., 1972. Seismic surface waves. Methods Comput. Phys. 11, 217–295.

Tanimoto, H., 1984. A simple derivation of the formula to calculate synthetic long-period seismograms in a heterogeneous earth by normal mode summation. Geophys. J. R. Astron. Soc. 77, 275–278.

Tanimoto, T., 1990. Long-wavelength S-wave velocity structure throughout the mantle. Geophys. J. Int. 100, 327–336.

Thomas, C., Igel, H., Weber, M., Scherbaum, F., Simulation of P-wave propagation in a heterogeneous spherical Earth: The influence of scatterers on the PKP wavefield. Geop. J. Int. 1999, in press.

Tromp, J., Dahlen, F.A., 1990. Summation of the born series for the normal modes of the Earth. Geophys. J. Int. 100, 527–533.

Weber, M., Davis, J.P., 1990. Evidence for a laterally variable lower mantle structure from P- and S-waves. Geophys. J. Int. 102, 231–255.

Woodhouse, J.H., 1983. The joint inversion of seismic waveforms for lateral variations in Earth structure and earthquake source parameters. In: Kanamori, H., Boschi, E. (Eds.), Proceedings of the Enrico Fermi International School of Physics, Vol. 85, North-Holland, Amsterdam, pp. 366–397.

Woodhouse, J.H., 1988. The calculation of eigenfrequencies and eigenfunctions of the free oscillations of the earth and the sun. In: Doornbos, D.J. (Ed.), Seismological Algorithms. Academic Press, London.

Woodhouse, J.H., Dziewonski, A.M., 1984. Mapping the upper mantle: three dimensional modelling of Earth structure by inversion of seismic waveforms. J. Geophys. Res. 89, 5953–5986.

Woodhouse, J.H., Dziewonski, A.M., 1987. Models of the upper and lower mantle from waveforms of mantle waves and body waves. EOS Trans. AGU 68, 356–357.

Yu, Y., Park, J., 1993. Upper mantle anisotropy and coupled-mode long-period surface waves. Geophys. J. Int. 114, 473–489.

Zhao, L., Dahlen, F.A., 1996. Mode-sum to ray-sum transformation in a spherical and an aspherical earth. Geophys. J. Int. 126, 389–412.